

## Activating ATRP Initiators to Incorporate End-Group Modularity into Photo-RAFT Polymerization

Karen Hakobyan, Christopher S. P. McErlean, and Markus Müllner\*



Cite This: <https://dx.doi.org/10.1021/acs.macromol.0c01697>



Read Online

ACCESS |



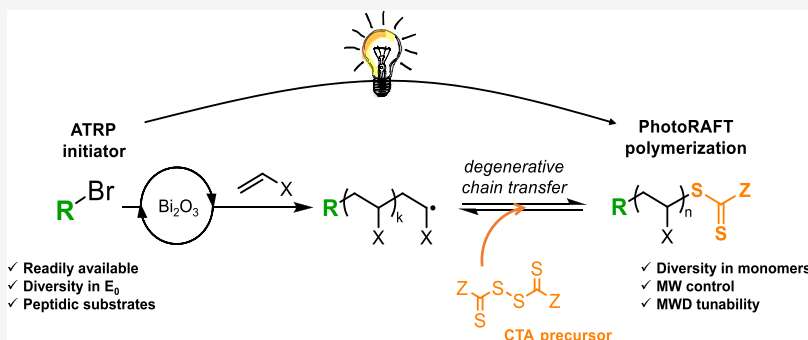
Metrics & More



Article Recommendations



Supporting Information



**ABSTRACT:** Heterogeneous photocatalysis is increasingly used in reversible deactivation radical polymerization (RDRP). In this study, we found that alkyl bromide redox chemistry typically found in atom transfer radical polymerization (ATRP) can be incorporated in concert with dithiocarbonyl disulfide chemistry into the reversible addition–fragmentation chain transfer (RAFT) process via bismuth oxide photocatalysis. This amalgamation of mechanisms introduces end-group modularity—a new layer of control—into RAFT polymers uniquely enabled by photoredox catalysis. We found that a diversity of functionality can be installed at the  $\alpha$ -end group via alkyl bromides, while the molecular weight distribution can be tuned seamlessly at the  $\omega$ -end group through the simultaneous addition of multiple disulfides.

### INTRODUCTION

Polymer research is increasingly moving toward the construction of macromolecules with rich functionality and with high control over molecular weight, giving well-defined architectures and nanostructures for applications in self-assembly and nanotherapeutics.<sup>1–3</sup> Both reversible addition–fragmentation chain transfer (RAFT) polymerization and atom transfer radical polymerization (ATRP) have proven to be robust and versatile methodologies to achieve these goals. There are, however, fundamental limitations associated with these, such as the relatively rigid end-group chemistry of RAFT, metal contamination from ATRP, and the frequent need for elevated temperatures for both processes. The application of modern photochemical methods to these important reactions has allowed them to be performed with greater functional group tolerance, helped minimize metal/catalyst contamination, and enabled reactions under ambient temperatures.<sup>4,5</sup>

The Cu<sup>II</sup>-amine complexes in conventional ATRP systems can be photoreduced to the active Cu<sup>I</sup> redox state by violet light and promote ATRP.<sup>6–9</sup> Iron tribromide acts analogously to Cu<sup>II</sup>-amine complexes under blue light irradiation and enables copper-free photoinitiated ATRP.<sup>10,11</sup> Research has increasingly been dedicated to avoiding metal contamination/Lewis acids from the polymerization process. A variety of

organic molecules, such as 10-phenylphenothiazine derivatives, have been reported as potent photoreductants to promote photo-ATRP in place of Cu<sup>I</sup>, or as photo-oxidants to promote the reaction upon activation with an external ligand.<sup>12–14</sup> Similarly, the application of iodide salts results in an iodine transfer polymerization (ITP) process, which in some cases can be performed with visible light irradiation in the absence of a catalyst.<sup>15,16</sup> Despite these developments in copper-free photo-ATRP, maintaining controlled polymerization without the specific activation–deactivation redox equilibrium provided by copper complexes presents a major challenge in polymer science.

In contrast, RAFT polymerization has seen the seamless incorporation of modern photochemical methods. This is because control of polymerization via degenerative chain transfer can be entirely separated from the light-driven initiation/propagation steps. With a predetermined chain-

Received: July 22, 2020

Revised: September 6, 2020

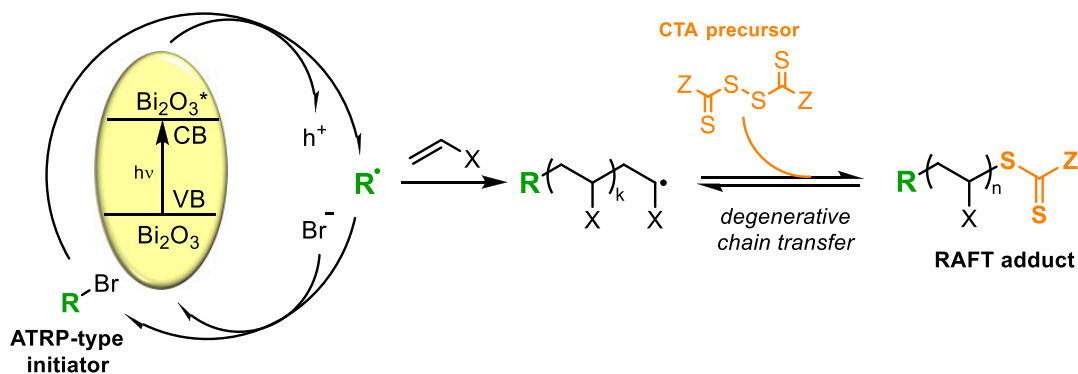


ACS Publications

© XXXX American Chemical Society

A

<https://dx.doi.org/10.1021/acs.macromol.0c01697>  
Macromolecules XXXX, XXX, XXX–XXX

Scheme 1. Proposed Mechanism of *In Situ* Conversion of “Photo-ATRP” to Photo-RAFT via Bismuth Oxide Photocatalysis

transfer agent (CTA), photo-RAFT polymerization can be performed through a variety of mechanisms and photocatalytic regimes, such as photoiniferter, energy transfer, electron transfer to the CTA, or electron transfer to an initiator.<sup>17</sup> RAFT CTAs contain a substituent attached to dithiocarbonyl disulfide at the  $\omega$ -end, called the “Z-group”, and an alkyl radical-derived “R-group” at the  $\alpha$ -end.<sup>18</sup> Methodologies exist to generate the “R-group” either prior to polymerization or *in situ* during the polymerization process. For example, it had been shown that performing the synthesis of a CTA in the presence of a monomer and an initiator leads to the corresponding RAFT polymerization in the same pot.<sup>19–21</sup> More recently, the Fors group was able to utilize a similar concept using hydridic C–H bonds as the source of the alkyl radicals.<sup>22</sup>

Our study describes the incorporation of alkyl bromide redox chemistry (typical of ATRP) into a RAFT process. By utilizing alkyl bromides as a source of alkyl radicals, it is possible to apply myriad photoreduction methodologies to chemoselectively reveal the “R-group” and initiate polymerization under mild conditions.<sup>23–25</sup> We previously reported a bismuth oxide-photocatalyzed system for PET-RAFT/MADIX and chose to adopt it for the photoreduction of alkyl bromides in this work.<sup>26,27</sup> Using this approach, we now demonstrate similar “R-group” tolerance to that afforded by traditional ATRP, even to the level of peptide substrates. We also leverage the modularity of the “Z-group” to tune the dispersity of polymers by adding a mixture of two disulfide precursors. By harnessing the known photochemistry of dithiocarbonyl disulfides, controlled polymerization is achieved, with modular end-group chemistry built into the process. In practice, this methodology circumvents the problems associated with copper-free photo-ATRP because the control of polymerization is not determined by the specific alkyl bromide redox equilibrium but rather by degenerative chain transfer onto disulfide (Scheme 1).

## EXPERIMENTAL SECTION

**Materials.** Bismuth oxide ( $\text{Bi}_2\text{O}_3$ , powder, 99.999% trace metals basis), iron(II,III) oxide ( $\text{Fe}_2\text{O}_3$ , powder, max 5  $\mu\text{m}$ , 95%), copper(I) oxide ( $\text{Cu}_2\text{O}$ , powder, max 7  $\mu\text{m}$ , 97%), bromoisobutyric acid (98.0+%), bromophenylacetic acid (racemic, 98%), benzyl bromide (98%),  $\alpha$ -D(+)-glucose pentaacetate (99%), bis(thiobenzoyl)disulfide (BisDTB, 95+%),  $\alpha$ -bromoisobutyl bromide (BiBB, 98%), *n*-butyl acrylate (*n*BA, 99+%), *tert*-butyl acrylate (*t*BA, 99+%), methyl methacrylate (MMA, 99%), *N*-isopropylacrylamide (NiPAAm, 97%), *N,N*-dimethylacrylamide (DMA, 99%), sodium hydride, (NaH, 60% dispersion in mineral oil), dodecanethiol (98+%), potassium ethyl xanthogenate (96%), tetrabutylammonium bromide

(TBAB, 98+%), carbon disulfide ( $\text{CS}_2$ , anhydrous), triisopropylsilane (TIPS, 98%), deuteriochloroform ( $\text{CDCl}_3$ , 99.8% atom D), and hexadeuteroacetone ( $(\text{CD}_3)_2\text{CO}$ , 99.9% atom D) were sourced from Sigma-Aldrich. For further characterization of bismuth oxide used in this project, refer to our previous work.<sup>26</sup> Diethyl ether (anhydrous), diisopropylcarbodiimide (DIC, 99+%), diisopropylethyl amine (DIPEA, 99%), triethylamine ( $\text{Et}_3\text{N}$ , 99%), biphenyl (99+%), 2-chlorotriethylchloride polystyrene resin (2CTC resin, 1% DVB, 1.33  $\text{mmol g}^{-1}$ ), diethylamine (99+%), ethanol ( $\text{EtOH}$ , E100), thionyl chloride (99+%), and piperidine (99+%) were sourced from Merck. Tungsten oxide ( $\text{WO}_3$ ) was sourced from Aithaca Chemical Corp. Trifluoroacetic acid (TFA, 99.5+%), hydrochloric acid (HCl, 32%), iodine ( $\text{I}_2$ , 99.5+%), sodium hydroxide (pellets), methanol ( $\text{MeOH}$ , 98%), and dichloromethane (DCM, 95+%) were sourced from Ajax. Methyl bromoacetate (MBA, 98%) was sourced from Fluka. *N,N*-Dimethylformamide (DMF, 99.8% by GC) was sourced from RCI LabScan and stored under molecular sieves. FMoc-*O*-*tert*-butyl-L-serine (FMoc-Ser(*t*Bu)-OH, 98+%), FMoc-*O*-*tert*-butyl-L-tyrosine (FMoc-Tyr(*t*Bu), 98+%), *N*/ $\beta$ -FMoc-*N*- $\alpha$ -Boc-L-lysine (FMoc-Lys-(Boc), 98+%), FMoc-L-proline (FMoc-Pro, 98+%), and ethyl (hydroxylimino)cyanoacetate (Oxymapure, 98+%) were purchased from Mimotopes.

All chemicals were used as received. Monomers (*n*BA, *t*BA, MMA, DMA) were passed through basic alumina prior to use except for NiPAAm, which was recrystallized from hexanes prior to use.

**Instrumentation.** Proton nuclear magnetic resonance ( $^1\text{H}$  NMR) spectra were recorded in deuterated solvents using a 300 MHz Bruker Avance system at 300 K and a 400 MHz Bruker Avance Bay III at 300 K.

Size-exclusion chromatography (SEC) measurements were performed on an UFLC Shimadzu Prominence SEC system with PhenogelTM columns (5  $\mu\text{m}$ , 104, and 105 Å) in DMAc with BHT and LiBr at 0.05 wt % as eluents at a flow rate of 1  $\text{mL min}^{-1}$  at 50 °C. SEC samples were dissolved and passed through a 220 nm nylon filter prior to injection. Apparent molecular weights were determined using a calibration procedure with near-monodisperse PMMA standards from Polymer Standards Service (PSS).

Semipreparative reverse-phase high-performance liquid chromatography (HPLC) was performed on a Waters Acquity system equipped with a Waters 2545 Quaternary Gradient Module, a Waters Fraction Collector III, a Waters 2707 Autosampler, and a Waters 2489 UV/Vis Detector with a Waters Sunfire prep C-18 (5  $\mu\text{m}$ ) column at a flow rate of 15  $\text{mL min}^{-1}$ . Three 0.5 mL injections of the product solution filtered through a 220 nm nylon filter ( $\text{H}_2\text{O}$  solution,  $\sim 27 \text{ mg mL}^{-1}$ ) was used.

Ultrahigh-performance liquid chromatography–mass spectrometry (UPLC–MS) was performed on a UFLC Shimadzu UPLC system coupled to a Shimadzu 2020 mass spectrometer (ESI) with a Waters Acquity BEH C-18 (1.7  $\mu\text{m}$ ) column at a flow rate of 0.6  $\text{mL min}^{-1}$ . UPLC–MS samples were dissolved and passed through a 220 nm nylon filter prior to injection.

Analytical reverse-phase ultrahigh-performance liquid chromatography (UPLC) was performed on a Waters Acquity UPLC system

with a Waters Acquity BEH C-18 (1.7  $\mu\text{m}$ ) column at a flow rate of 0.6 mL  $\text{min}^{-1}$ . UPLC samples were dissolved and passed through a 220 nm nylon filter prior to injection.

Cyclic voltammetry (CV) was performed using a Bioanalytical Systems Electrochemical Analyzer. The electrolyte solution (( $\text{Bu}_4\text{N}$ )- $\text{PF}_6$ , 0.1 M in acetonitrile) was sparged with argon before use. The voltammogram was recorded using a glassy carbon working electrode (1.5 mm diameter), a platinum wire as the counter electrode, and an Ag/Ag<sup>+</sup> wire reference electrode was used. Ferrocene was added as an internal standard upon completion of each experiment. All potentials are quoted in mV vs Fc<sup>+</sup>/Fc (calibrated as  $E^\circ = 450$  mV vs Ag/Ag<sup>+</sup>).

Electrospray ionization mass spectrometry (ESI-MS) was performed on a Thermo VelosPro Orbitrap mass spectrometer. Samples were infused via a syringe pump at 10  $\mu\text{L min}^{-1}$  with the standard electrospray ionization source. The capillary was set to a temperature of 330  $^\circ\text{C}$ , a potential of 4.5 kV, and with the nebulizer pressure at 10 psi. Orbitrap was run in full scan mode (or high mass mode when scanning up to 4000  $m/z$ ) with a resolving power of 100,000, and a lock mass of dioctylphthalate ( $[\text{M} + \text{H}]^+ 391.284286$   $m/z$ ,  $[\text{M} + \text{Na}]^+ 413.266230$   $m/z$ ) was used for calibration.

Resin loading calculation was performed via UV–vis spectrophotometry. To calculate amino acid loading, the dried resin ( $\sim 1$  mg) was added to a solution of piperidine in DMF (3 mL, 20% v/v). This was left to react for at least 15 min. The UV–visible spectrum of the filtrate was then obtained on an Agilent Technologies Cary 5000 spectrometer at room temperature. The absorbance value at 290 nm was taken against a 20% piperidine blank (dibenzofulvene–piperidine adduct has an experimentally determined value for molar absorptivity in DMF @301 nm,  $\epsilon = 7800$  L  $\text{mol}^{-1} \text{cm}^{-1}$ ).

Nonlinear curve fitting of molecular weight distributions was performed on OriginPro 8.6 software using the Levenberg–Marquardt algorithm against bi-Gaussian curves.

**Synthesis of Chain-Transfer Agents and Initiators.** *Synthesis of Bis(dodecylsulfanylthiocarbonyl) Disulfide, BisTTC.* *n*-Dodecanethiol (5.13 g, 25 mmol) was added dropwise to a stirred suspension of sodium hydride (60% dispersion in mineral oil) (1.16 g, 26 mmol) in dry diethyl ether (50 mL) over 10 min at around 5  $^\circ\text{C}$ . The evolution of hydrogen production was observed, and a thick white slurry of sodium thiododecylate was generated. The reaction mixture was cooled to 0  $^\circ\text{C}$ , and carbon disulfide (2.0 g, 26 mmol) was added dropwise. Iodine (2.1 g, 25 mmol) was then added portionwise, and the suspension was stirred for 1 h at room temperature. The yellow filtrate was washed with a solution of sodium thiosulfate to remove excess iodine, dried over with sodium sulfate, and concentrated under vacuum. The residue was then purified under flash chromatography on silica gel (hexanes). A yellow solid was obtained (12.1 g, 83% yield); mp 32–35  $^\circ\text{C}$ ;  $^1\text{H NMR}$  (300 MHz,  $\text{CDCl}_3$ )  $\delta(\text{ppm})$ : 3.32 (t,  $J = 7.5$  Hz, 4H), 1.71 (p,  $J = 6.9$  Hz, 4H), 1.55–1.15 (m, 36H), 0.90 (t,  $J = 7.2$  Hz, 6H) (for full spectrum, see Supporting Information Figure S1-1).

*Synthesis of Dioxanthenone, BisXan.* Potassium ethyl xanthogenate (2.00 g, 12.5 mmol) was dissolved in methanol (50 mL, 0.25 M), and iodine (1.60 g, 6.25 mmol) was added portionwise at room temperature. The solution was then concentrated under vacuum and then precipitated in water. The residue was washed with saturated aqueous sodium thiosulfate and then water and dried under vacuum. A light-yellow solid was obtained (1.5 g, quantitative); mp 28–34  $^\circ\text{C}$ ;  $^1\text{H NMR}$  (300 MHz,  $\text{CDCl}_3$ )  $\delta(\text{ppm})$ : 4.64 (q,  $J = 7.2$  Hz, 4H), 1.37 (t,  $J = 7.2$  Hz, 6H) (for full spectrum, see Supporting Information Figure S1-2).

*Synthesis of Methyl Bromophenylacetate, MBPA.* Bromophenylacetic acid (5.38 g, 50 mmol) was dissolved in a solution of concentrated sulfuric acid in methanol (50 mL, 1.5% v/v) and stirred under reflux for 1 h. The solution was then cooled to room temperature and concentrated under vacuum. The residue was then dissolved in diethyl ether and washed with 10% aqueous sodium bicarbonate, washed with brine, dried under magnesium sulfate, and concentrated again under vacuum. A slightly yellow oil was obtained (5.5 g, 24 mmol, 96% yield)  $^1\text{H NMR}$  (300 MHz,  $\text{CDCl}_3$ )  $\delta(\text{ppm})$ :

7.60–7.52 (m, 2 H), 7.40–7.34 (m, 3 H), 5.28 (s, 1 H), 3.79 (s, 3 H) (for full spectrum, see Supporting Information Figure S1-3).

*Synthesis of Methyl Bromoisobutyrate, MBiB.* Bromoisobutyric acid (4.17 g, 25 mmol) was dissolved in a solution of concentrated sulfuric acid (0.75 mL) and methanol (50 mL) and stirred under reflux for 2 h. The solution was then cooled to room temperature and concentrated under vacuum. The residue was dissolved in diethyl ether and washed with 10% aqueous sodium bicarbonate, washed with brine, dried under magnesium sulfate, and concentrated again under vacuum. A colorless oil was obtained (4.2 g, 23 mmol, 93% yield)  $^1\text{H NMR}$  (300 MHz,  $\text{CDCl}_3$ )  $\delta(\text{ppm})$ : 3.78 (s, 3H), 1.93 (s, 6H) (for full spectrum, see Supporting Information Figure S1-4).

*Solid-Phase Peptide Synthesis of BiB-SPKYS-OH.* To pretreat the resin for peptide synthesis, the CTC resin (500 mg, max reactive units 0.666 mmol, 1.33 mmol/g) was agitated in a solution of thionyl chloride in DCM (8 mL, 5% v/v) at room temperature for 2 h after which was washed with a solution of DIPEA in DCM (7  $\times$  5 mL) and dichloromethane (3  $\times$  5 mL).

A portion of the CTC resin (100 mg, 0.13 mmol reactive sites, 1.33 mmol/g) was then agitated in a solution of FMoc-Ser(*t*Bu)-OH (204 mg, 0.53 mmol, 4 equiv) and DIPEA (137 mg, 1.06 mmol, 8 equiv) in DCM (4.3 mL of 0.125 M amino acid) for 16 h at room temperature and then washed with DCM (5  $\times$  5 mL). The resin was then agitated in a solution of DCM, DIPEA, and methanol (5 mL, 17:2:1 v/v/v, respectively) for 30 min and then washed again with DCM (5  $\times$  5 mL) and diethyl ether (3  $\times$  5 mL) and then dried under vacuum. Resin loading was found to be 48% by the conditions outlined previously.

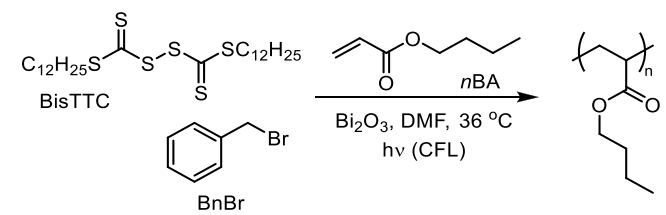
The following deprotection, coupling, and capping cycle was repeated for each amino acid. The rest of the coupled resin was swelled in DCM at room temperature and then washed with DMF (5  $\times$  5 mL). This was then agitated in a solution of piperidine in DMF ( $\sim 3$  mL, 20% v/v) for 15 min and then washed with DMF (3  $\times$  3 mL). The deprotected resin was then agitated in a solution of FMoc-protected amino acid (0.27 mmol, 4 equiv, 124 mg for FMoc-Tyr(*t*Bu)-OH, 126 mg for FMoc-Lys(Boc)-OH, 91 mg for FMoc-Pro-OH, 102 mg for FMoc-Ser(*t*Bu)-OH), DIC (34 mg, 0.27 mmol, 4 equiv), and OxymaPure (38 mg, 0.27 mmol, 4 equiv) in DMF (1.3 mL) at room temperature for 1 h. This was then washed with DMF (5  $\times$  5 mL) and DCM (3  $\times$  5 mL). The coupled resin was then agitated in a solution of acetic anhydride and DIPEA in DMF (3 mL, 2.5 and 5% v/v, respectively) for 15 min.

Upon coupling of the final amino acid, capping, and N-terminus deprotection, the resin was agitated in a solution of bromoisobutyryl bromide (BiBB) and DIPEA in DMF (5 mL, 2.5 and 5% v/v, respectively) for 1 h at room temperature and then washed with DMF (5  $\times$  5 mL) and DCM (5  $\times$  5 mL).

The resin-functionalized, side chain-protected product was washed with DCM (10  $\times$  5 mL). This was then agitated in a solution of TFA and TIPS in deionized water (5 mL, 90 and 5% v/v, respectively) at room temperature for 2 h. The filtrate was then concentrated under nitrogen flow, and the product was precipitated twice in diethyl ether. Upon purification by HPLC and lyophilization, a colorless solid was obtained (32 mg, 70% resin yield, 93% stepwise yield)  $^1\text{H NMR}$  (500 MHz,  $\text{D}_2\text{O}$ )  $\delta(\text{ppm})$ : 7.09 (d,  $J = 8.5$  Hz, 2H), 6.77 (d,  $J = 8.5$  Hz, 2H), 4.69–4.66 (m, 1H), 4.62 (dd,  $J = 9.3, 5.7$  Hz, 1H), 4.38 (t,  $J = 4.5$  Hz, 1H), 4.33 (dd,  $J = 8.3, 6.0$  Hz, 1H), 4.16 (dd,  $J = 8.4, 6.4$  Hz, 1H), 3.94–3.76 (m, 5H), 3.66 (dt,  $J = 10.1, 6.9$  Hz, 1H), 3.09 (dd,  $J = 14.0, 5.7$  Hz, 1H), 2.92–2.83 (m, 3H), 2.23–2.12 (m, 1H), 1.95 (p,  $J = 6.8$  Hz, 2H), 1.88 (d,  $J = 5.3$  Hz, 6H), 1.76–1.66 (m, 1H), 1.66–1.52 (m, 4H), 1.36–1.16 (m, 2H) (for full spectrum, see Supporting Information Figure S9-5 with two-dimensional spectra in Figures S9-6–S9-8).

**Polymerization.** *General Procedure for the Synthesis of Poly(*n*-butyl acrylate), PnBA.* In a typical experiment, a solution of bis(dodecylsulfanylthiocarbonyl) disulfide (1 equiv) in *n*-butyl acrylate (40 equiv) was added to a solution of alkyl bromide (2 equiv) in DMF (10 M monomer concentration, 0.8 monomer/solvent mole ratio) in a 4 mL vial. Bismuth oxide (0.2 equiv) was added to the solution. The reaction vial was sealed with a septum and degassed



Table 1. Proof-of-Concept System Using *n*-Butyl Acrylate (*n*BA): Optimization and Control Experiments<sup>a</sup>


| entry | [ <i>n</i> BA]:[BnBr]:[BisTTC]:[Bi <sub>2</sub> O <sub>3</sub> ]                  | conversion, <sup>b</sup> reaction time                                 | <i>M</i> <sub>n,NMR</sub> (g mol <sup>-1</sup> ) <sup>c</sup> | <i>M</i> <sub>n,SEC</sub> (g mol <sup>-1</sup> ) <sup>d</sup> | <i>Đ</i> <sup>e</sup>                     |
|-------|---|--|---|---|---|
| 1     | 100:1:0:0.2   | 62%, 14 h  | 8300  | 71,000  | 2.11                                      |
| 2     | 40:2:1:0.2  | 99+%, 7.5 h;<br>99+%, 5 h;<br>99+%, 5 h                                | 5500;<br>5500;<br>5500  | 6100;<br>6200;<br>6100  | 1.16;<br>1.18;<br>1.14                    |
| 3     | 40:2:1:0  | 0%, 7.5 h;<br>0%, 24 h;<br>0%, 24 h                                    |   | 500 (disulfide);<br>500 (disulfide);<br>500 (disulfide)       |   |
| 4     | 200:2:1:0.28;<br>200:2:1:0.08;<br>200:2:1:0.04;<br>200:2:1:0.02;<br>200:2:1:0.004 | 99+%, 14 h;<br>99+%, 14 h;<br>99+%, 14 h;<br>99+%, 14 h;<br>99+%, 14 h | 26,000;<br>26,000;<br>26,000;<br>26,000;<br>26,000            | 26,000;<br>26,300;<br>26,500;<br>26,200;<br>26,600            | 1.18;<br>1.15;<br>1.17;<br>1.16;<br>1.18; |
| 5     | 40:0:1:0.2  | 18%, 14 h;<br>23%, 14 h;<br>22%, 14 h                                  | 1300;<br>1500<br>1500   | 1800;<br>2300<br>2400   | 1.06;<br>1.08;<br>1.08                    |
| 6     | 40:0.1:1:0.2;<br>40:0.5:1:0.2;<br>40:1:1:0.2;<br>40:4:1:0.2                       | 32%, 14 h;<br>99+%, 14 h;<br>99+%, 14 h;<br>99+%, 14 h                 |   | 2400;<br>5200;<br>6300;<br>4800;                              | 1.21<br>1.21<br>1.12<br>1.11              |
| 7     | 100:2:1:0.2;<br>400:2:1:0.2;<br>800:2:1:0.2;<br>1600:2:1:0.2                      | 99+%, 5 h;<br>99+%, 5 h;<br>94%, 5 h;<br>72%, 5 h                      | 13,200;<br>51,600;<br>96,800;<br>148,000                      | 11,600;<br>51,500;<br>86,300;<br>126,800                      | 1.14;<br>1.13;<br>1.18;<br>1.27           |

<sup>a</sup>All reactions were performed in DMF (10 M monomer concentration, 0.8 monomer/solvent mole ratio). <sup>b</sup>Calculated from changes in characteristic NMR integrals. <sup>c</sup>Calculated from the product of conversion and [*n*BA]:[BisTTC]. <sup>d</sup>Calculated from SEC with PMMA calibration. <sup>e</sup>Calculated from SEC with  $\bar{D} = M_w/M_n$ .

by sparging with argon for 15 min. The mixture was irradiated under CFL (23 W, 1610 lm, 4 mL vial held 1.5 cm away,  $7.6 \pm 0.8$  mW cm<sup>-2</sup>) at 36 °C for 5 h. The catalyst was removed via centrifugation (2000 rcf), and the polymer was precipitated twice in a methanol/water mixture (10% v/v). The swollen precipitate was dissolved in acetone, further purified under dialysis (2000 Da cutoff) in acetone, and concentrated under vacuum. A light-yellow viscous liquid was obtained. Residual bismuth oxide in the reaction vessel and on stirrer bar was removed by immersion into a hydrochloric acid (3 M) bath for 2 h.

Polymerization kinetics were measured from the reaction performed under the conditions outlined above. Small aliquots (<50 μL) from the reaction mixture were taken under an argon atmosphere with subsequent sparging under argon for 2 min. The samples were analyzed for conversion by <sup>1</sup>H NMR using a combination of two methods: first, by the integration of vinyl resonances of the monomer against an internal standard and, second, by the integration of vinyl resonances of the monomer against a region containing resonances from both the monomer and corresponding polymer. The NMR samples were concentrated under nitrogen flow and then analyzed under SEC with the conditions outlined above.

**Results and Discussion.** We began our work by attempting to perform photo-ATRP using the heterogeneous photocatalytic protocol that we had previously demonstrated to be viable in a photo-RAFT setting.<sup>26</sup> However, no noticeable molecular weight control and only broad molecular weight distributions (MWDs) were observed (Table 1, entry 1). We varied several parameters with no discernable improvement and concluded that controlled photo-ATRP

using this methodology was unlikely to be achieved (see Supporting Information S2). We rationalized this outcome as resulting from slow deactivation of the reactive species in the ATRP equilibrium with respect to the activated species. However, knowing that dithiocarbonyl disulfides can be effective precursors to CTA propagating species, we proposed that the alkyl bromide reduction under bismuth oxide photocatalysis could establish photo-RAFT *in situ*.

In a proof-of-concept polymerization of *n*-butyl acrylate, *n*BA, (Figure 1), we found that CFL irradiation in the presence of bismuth oxide, Bi<sub>2</sub>O<sub>3</sub>, promoted controlled photopolymerization (Table 1, entry 2). More importantly, the alkyl substituent and trithiocarbonate were found by nuclear magnetic resonance (NMR) end-group analysis (Figure 1A) to be incorporated, which agreed well with the expected molecular weight by conversion. A kinetics experiment revealed uniform molecular weight evolution (Figure 1B), and the kinetic plot followed a pseudo-first-order rate law as expected for RDRP (inset of Figure 1B). Electrospray ionization mass spectrometry (ESI-MS) (Figure 1C) revealed that the intended adduct was formed with multiple repeating peaks corresponding to various ions associated with the same general adduct structure (see Supporting Information Figure S3-1 and Table S3-1).

The requirement of photocatalysis was confirmed in a control experiment (Table 1, entry 3), in which the absence of Bi<sub>2</sub>O<sub>3</sub> resulted in no polymerization. Pleasingly, we found that the catalyst loading could be substantially reduced without significantly affecting the MWD (Table 1, entry 4, and Supporting Information Figure S3-3). Interestingly, when the alkyl bromide was omitted in this reaction (Table 1, entry 5), photopolymerization still occurred, albeit without the incorporation of the “R-group” from the missing alkyl bromide

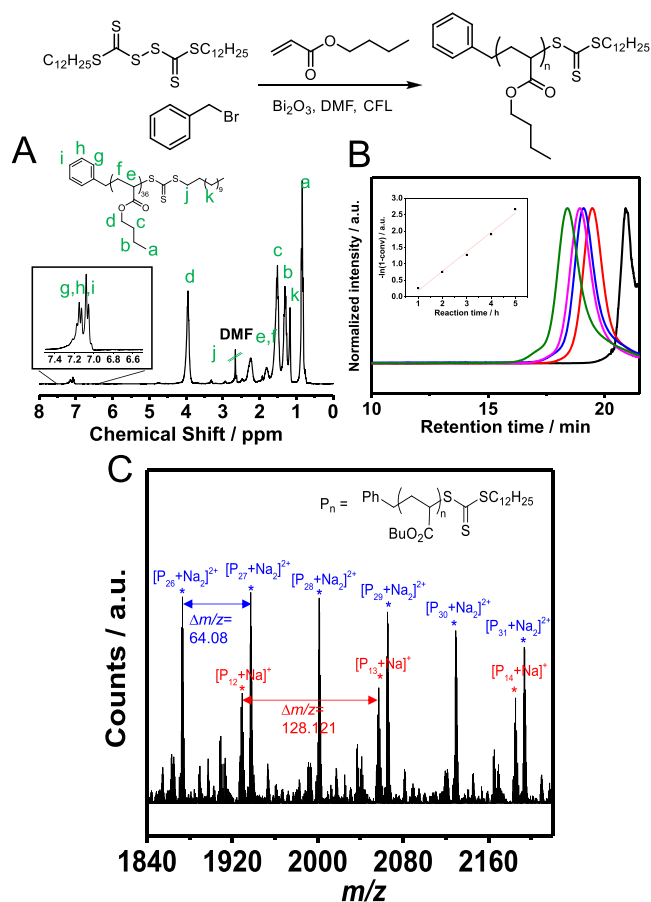


**Figure 1.** Proof-of-concept system using *n*BA, benzyl bromide, and bis(dodecylsulfanylthiocarbonyl) disulfide (BisTTC). (A)  $^1\text{H}$  NMR ( $d_6$ -acetone, 300 MHz) of the adduct polymer. (B) Evolution of the MWD over the course of the reaction by SEC (DMAc,  $1\text{ mL min}^{-1}$ ,  $50\text{ }^\circ\text{C}$ ), with the corresponding kinetics in the inset. (C) Shortened range ( $m/z = 1840\text{--}2200$ ) of the ESI mass spectrum (MeOH) of the adduct polymer.

initiator. We attribute this polymerization to the redox activity of the disulfide and will report further findings on this subject in due course elsewhere. Supporting our hypothesis, decreasing the alkyl bromide stoichiometry (Table 1, entry 6) resulted in a largely unchanged MWD relative to the previous conditions (see Supporting Information Figures S3-4 and S3-5). When an alkyl halide that is inert to bismuth oxide photocatalysis (e.g., benzyl chloride) was used, the characteristic benzylic “R-group” incorporation was absent (see Supporting Information Figure S3-6). Collectively, these outcomes demonstrate the fundamental involvement of alkyl bromide mesolysis as the crucial step in the initiation and subsequent “R-group” incorporation using this new methodology.

For those proof-of-concept experiments, we maintained a rather low target DP to facilitate characterization via ESI-MS and  $^1\text{H}$  NMR. The methodology is however suitable for the generation of higher-molecular-weight polymers (Table 1, entry 7) while maintaining relatively monodisperse MWDs. Termination, however, seemed to become increasingly prominent in the polymerization as the target molecular weight increased. This was reflected in tailing and chain–chain coupling indicated in the molecular weight distributions (see Supporting Information Figures S3-7 and S3-8).

To better understand the behavior of our system and confirm that a RAFT adduct has formed in polymerization, chain extension was performed. The *Pn*BA macro-CTA made via our methodology was mixed with *tert*-butyl acrylate (i.e., the subsequent block forming monomer) and exposed to visible light. A clear chain extension was

achieved (see Supporting Information S4) via a photoiniferter process.

The success of benzyl bromide in our model system led us to explore the scope of alkyl bromides that can be employed. We focused mostly on substituted alkyl bromides that have previously been used in ATRP. Electrochemical measurements showed significant differences in reduction potentials across these alkyl bromides (see Supporting Information S5) but suggested that each alkyl bromide should be incorporated as intended via our proposed mechanism. Indeed, each alkyl bromide investigated (Table 2, entries 1–4) was incorporated into the  $\alpha$ -end of each sample of *Pn*BA with little variation in MWD (for complete characterization, see Supporting Information S6). Even the electron-rich sugar bromide, tetraacetylglucosyl bromide (TAGB), which would normally not be used as a typical ATRP initiator, demonstrated similar reactivity (Table 2, entry 5).

The key finding from these reactions using different alkyl bromide initiators is that the redox equilibrium of the alkyl bromide seems to be of minor importance to the overall process. Instead, it is the disulfide that imparts control in this polymerization. Consequently, this greatly expands the scope of alkyl bromide initiators that can be employed beyond those currently used in ATRP.

Having investigated the role of the “R-group”, we switched our attention to the “Z-group”. RAFT polymerization is suitable for a wide variety of monomers through the application of diverse dithiocarbonyl “Z-group” substituents (Table 2, entries 6 and 7). We imagined that a similar versatility in monomer scope could be afforded by our methodology.

Surprisingly, we found that controlled polymerization using bis(thiobenzoyl)disulfide (BisDTB) was not as straightforward as anticipated. We observed significant termination events due to dithiobenzoate decomposition during polymerization (see Supporting Information Figure S7-1). Nonetheless, a variety of electron-deficient alkenes underwent controlled polymerization using our methodology (Table 2, entries 6–9). While this process was compatible with dioxanthogen (BisXan), less activated monomers (LAMs) did not undergo polymerization. We have previously shown that LAMs can undergo radical polymerization under photoreducing conditions with a dithiocarbonyl compound, but in this instance, the presence of an  $\alpha$ -heteroatom in the propagating species likely results in competitive bromide elimination and termination. These outcomes provide further evidence that free radical polymerization initiated by the alkyl bromide must be occurring prior to degenerative chain transfer onto a dithiocarbonyl disulfide.

In each of the preceding polymerizations, we had focused on minimizing MWD across different monomer classes. However, we realized that “Z-group” modularity could serve as a very simple way of fine tuning the MWD for a variety of polymers, which is an important aspect of controlled radical polymerizations.<sup>28</sup> The ability to access greater dispersity (and also tune other parameters in the MWD) can result in beneficial physical/self-assembly properties, such as higher order–disorder temperatures, more pronounced phase separation in the bulk with a wider domain spacing, and improved processability (through favorable rheological characteristics such as larger extensional viscosity).<sup>29–31</sup> In a conventional RAFT setting, the dispersity depends on the chain-transfer constant ( $C_s$ ) of the CTA, which is influenced most strongly by the “Z-group” substituent.<sup>32</sup> This provides a discrete change in dispersity but cannot be used to continuously tune dispersity in a conventional batch setting. Recently, Anastasaki and co-workers introduced a method to easily control the dispersity of RAFT polymers through the combination of two CTAs with differing  $C_s$  values.<sup>33</sup>

Due to end-group modularity of our method, we anticipated that it would be straightforward to add two (or even multiple) “Z-group” precursor disulfides to the reaction mixtures. In practice, we synthesized various samples of *Pn*BA with a comparable number-average molecular weight but with distinctly different MWDs (Figure 2). Thus, we added varying amounts of dioxanthogen and bis(dodecylsulfanylthiocarbonyl) disulfide to the reaction mixtures (see Supporting Information S8). Monomodal MWDs were maintained

Table 2. Scope of Alkyl Bromides, Monomers, and Dithiocarbonyl Disulfides<sup>a</sup>

| Entry          | Adduct structure | [M]: [RBr]: [CTA]:<br>[Bi <sub>2</sub> O <sub>3</sub> ],<br>monomer, RBr,<br>CTA | Conversion, <sup>b</sup><br>reaction time | M <sub>n</sub> , NMR<br>(g mol <sup>-1</sup> ) <sup>c</sup> | M <sub>n</sub> , SEC<br>(g mol <sup>-1</sup> ) <sup>d</sup> | Đ <sup>e</sup> |
|----------------|------------------|--|---|---|---|----------------|
| 1              |                  | 40: 2: 1: 0.2,<br><i>n</i> BA, BnBr, BisTTC                                      | 99+%, 5 h                                 | 5,500   | 6,100   | 1.18           |
| 2              |                  | 40: 2: 1: 0.2<br><i>n</i> BA, MBPA,<br>BisTTC                                    | 99+%, 14 h                                | 5,600   | 6,100   | 1.16           |
| 3              |                  | 40: 2: 1: 0.2<br><i>n</i> BA, MBA, BisTTC  | 99+%, 14 h                                | 5,500   | 6,100   | 1.15           |
| 4              |                  | 40: 2: 1: 0.2<br><i>n</i> BA, MBiB, BisTTC                                       | 99+%, 14 h                                | 5,600   | 5,700   | 1.21           |
| 5              |                  | 40: 2: 1: 0.2<br><i>n</i> BA, TAGB, BisTTC                                       | 99+%, 14 h                                | 5,700   | 9,100   | 1.10           |
| 6 <sup>f</sup> |                  | 40: 2: 1: 0.2<br>MMA, MBPA,<br>BisDTB  | 90%, 14 h                                 | 3,900   | 5,400   | 1.43           |
| 7              |                  | 100: 2: 1: 0.2<br>DMA, MBPA,<br>BisXan   | 70%, 14 h                                 | 7,400   | 23,400  | 1.54           |
| 8 <sup>g</sup> |                  | 100: 2: 1: 0.2<br>MMA, MBiB,<br>BisTTC   | 70%, 2.5 h                                | 7,300   | 9,000   | 1.26           |
| 9              |                  | 100: 2: 1: 0.2<br>NiPAAm, MBPA,<br>BisTTC  | 88%, 14 h                                 | 10,400  | 11,900  | 1.13           |

<sup>a</sup>All reactions were performed in DMF (10 M monomer concentration, 0.8 monomer/solvent mole ratio) unless otherwise indicated. <sup>b</sup>Calculated from changes in characteristic NMR integrals. <sup>c</sup>Calculated from the product of conversion and [M]:[CTA]. <sup>d</sup>Calculated from SEC with PMMA calibration. <sup>e</sup>Calculated from SEC with  $\bar{D} = M_w/M_n$ . <sup>f</sup>Performed in DMF (5 M monomer concentration, 0.4 monomer/solvent mole ratio). <sup>g</sup>Performed in DMF (2 M monomer concentration, 0.16 monomer/solvent mole ratio).

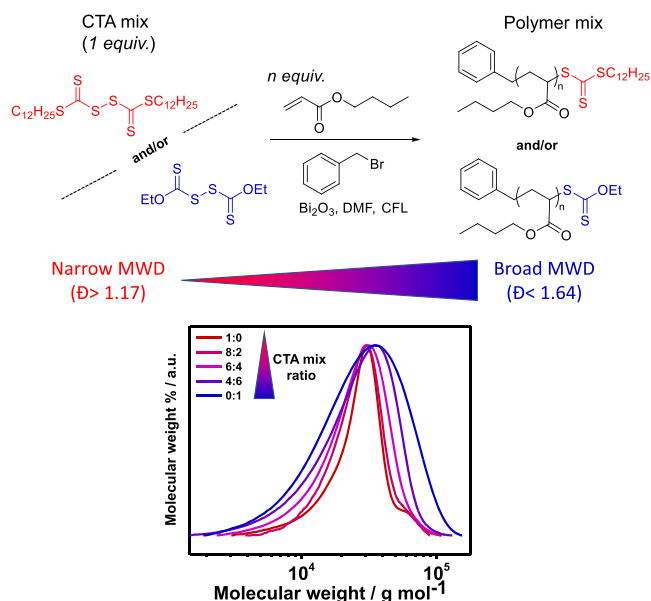


**Figure 2.**  $PnBA_{200}$  with a range of dispersity ( $1.18 < \bar{D} < 1.64$ ) synthesized through the addition of various ratios of bis-(dodecylsulfanylthiocarbonyl) disulfide and dioxanogen as CTAs. Target DP for each polymerization was 200, i.e., a target  $M_n$  of  $26,000 \text{ g mol}^{-1}$ , and all reactions were run to completion (99%+ monomer conversion).

with the mixtures of RAFT adducts due to degenerative chain transfer. We envisage that a wider range of MWDs can be achieved this way using an additive dithiocarbonyl disulfide of an even lower  $C_s$  value. Further exploration of this topic is ongoing.

To illustrate the applicability of our methodology, we used peptide-functionalized alkyl bromides to quantitatively generate functionalized peptide–polymer hybrids. Peptide–polymer hybrids are an important class of functional macromolecules. Peptide structures can specifically target disease-modifying proteins, while polymers can aid in their therapeutic delivery.<sup>34</sup> Furthermore, the incorporation of peptides into macromolecular hybrids can provide an excellent platform for self-assembly due to their variety of noncovalent interactions and stereoregularity.<sup>35</sup> Their synthesis often requires careful consideration given their wide array of composition reflecting in the number of possible side reactions that can occur. Often, a “grafting from” approach is opted for in their synthesis. In doing so, the functionality is incorporated into polymerization itself, namely, in the CTA or initiator. This harnesses the specific requirements of living polymerization to ensure near-quantitative installation of the functionality. RAFT polymerization displays excellent functional group tolerance and has been used in the generation of some protein–polymer conjugates.<sup>36,37</sup> However, some nucleophiles present in peptides, such as free amines, can lead to cleavage of the dithiocarbonyl functional group key to RAFT.<sup>38</sup> Because our methodology preinstalls alkyl bromide functionality, we reasoned that peptide-containing alkyl bromides would make suitable substrates.<sup>39–41</sup>

To this end, we synthesized an *N*-terminal bromoisobutyryl amide of Ser-Pro-Lys-Tyr-Ser-OH (BiB-SPKYS-OH) (see Supporting Information S9) via solid-phase peptide synthesis (SPPS). The choice of the peptide was due to the presence of nucleophilic (serine and lysine) and redox-active (lysine and tyrosine) residues, albeit with no cysteine present. Upon full deprotection and purification, the peptide-based initiator was used in our photopolymerization protocol (Figure 3). With no changes in reaction conditions, we were able to graft *n*BA from the model peptide. The incorporation of the peptide was confirmed by the presence of resonance associated with tyrosine in the  $^1\text{H}$  NMR spectra of the purified product (Figure 3A). The polymer was found to have a similarly uniform MWD as the previous samples of *Pn*BA with variable  $\alpha$ -ends by SEC (Figure 3B). It is

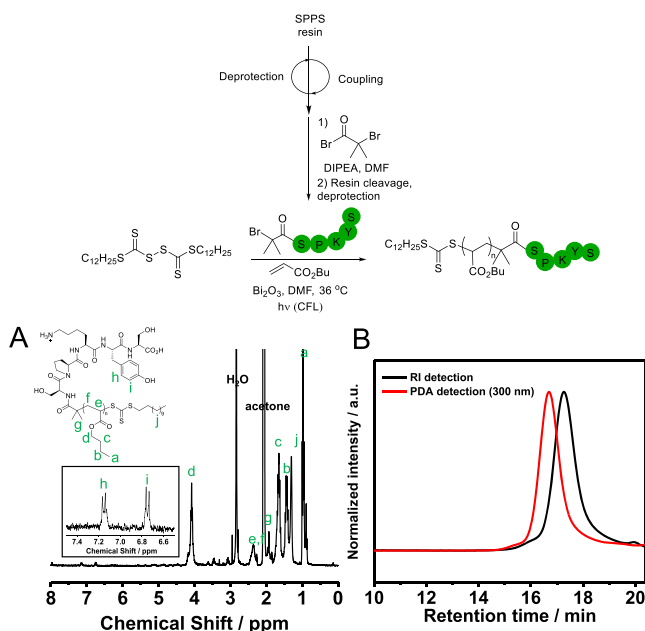


**Figure 3.** Peptidic alkyl bromide initiator BiB-Ser-Pro-Lys-Tyr-Ser-OH (BiB-SPKYS) synthesized by SPPS and the resulting peptide–polymer hybrid SPKYS-g- $PnBA_{37}$ . (A)  $^1\text{H}$  NMR ( $d_6$ -acetone, 300 MHz) spectrum of the hybrid polymer. (B) SEC elugram (DMAC,  $1 \text{ mL min}^{-1}$ ,  $50^\circ\text{C}$ ) of the hybrid polymer under RI (black) and PDA detection (red)  $M_n = 16,000 \text{ g mol}^{-1}$ ,  $\bar{D} = 1.12$ .

interesting to note the wide disparity of what is expected by both conversion and end-group analysis ( $<7000 \text{ g mol}^{-1}$ ) and by what is apparent in the SEC even with a relatively monodisperse MWD. We attribute this to a potentially large effect of the highly polar end group has on the hydrodynamic volume in the eluent used for SEC. ESI-MS of the hybrid (see Supporting Information Figure S9-9) provided proof that the peptide was indeed incorporated into the  $\alpha$ -end of the polymer.

**Conclusions and Outlook.** We have developed a simple method for installing end-group modularity into RAFT polymerization. This was achieved by utilizing the redox chemistry of alkyl bromides under heterogeneous photocatalysis. We have explored different ways in which such modularity could be beneficial in polymer synthesis. Modularity at the  $\omega$ -end (the “Z-group”) can allow for continuous tuning of dispersity in a RAFT context, while modularity at the  $\alpha$ -end (the “R-group”) allowed the installation of a wide variety of functionalities, including peptides.

Alkyl bromides were a natural choice of precursors for the “R-group” due to their commercial availability, previous use in ATRP, and their known reactivity under heterogeneous catalysis. There is, however, a plethora of substrate types that can undergo chemo-selective cleavage under photoredox catalysis to reveal potential “R-groups”.<sup>23–25</sup> The key considerations governing the choice of substrate is whether the initiation is fast relative to the rate of propagation and, less obviously, whether the generated radical can undergo degenerative chain transfer in the “pre-equilibrium” phase of the RAFT process.

## ■ ASSOCIATED CONTENT

### Supporting Information

The Supporting Information is available free of charge at <https://pubs.acs.org/doi/10.1021/acs.macromol.0c01697>.

Information on methods and additional experiments and characterization of our methodology (PDF)



## AUTHOR INFORMATION

### Corresponding Author

Markus Müllner — Key Centre for Polymers and Colloids,  
School of Chemistry, The University of Sydney, Sydney, NSW  
2006, Australia; The University of Sydney Nano Institute  
(Sydney Nano), Sydney, NSW 2006, Australia;  
orcid.org/0000-0002-0298-554X;  
Email: markus.muellner@sydney.edu.au

### Authors

Karen Hakobyan — Key Centre for Polymers and Colloids,  
School of Chemistry, The University of Sydney, Sydney, NSW  
2006, Australia

Christopher S. P. McErlean — School of Chemistry, The  
University of Sydney, Sydney, NSW 2006, Australia;  
orcid.org/0000-0001-8930-7495

Complete contact information is available at:

<https://pubs.acs.org/10.1021/acs.macromol.0c01697>

### Author Contributions

All authors have given approval to the final version of the manuscript.

### Funding

M.M. acknowledges the Australian Research Council for support (DE180100007).

### Notes

The authors declare no competing financial interest.

## ACKNOWLEDGMENTS

We thank Dr. Nicholas Proschogo and the Mass Spectrometry Facility for his support in mass spectrometry characterization. We thank A/Prof. Deanna D'Alessandro and Xiaochen Fu for their support in electrochemical characterization. We thank Prof. Richard Payne, Jason Johansen-Leete, and Wendy Tran for their support in peptide synthesis and characterization.

## ABBREVIATIONS

ATRP, atom transfer radical polymerization; CRP, controlled radical polymerization; CTA, chain-transfer agent; FRP, free radical polymerization; MWD, molecular weight distribution; RAFT, reversible addition–fragmentation chain transfer

## REFERENCES

- (1) Grubbs, R. B.; Grubbs, R. H. 50th Anniversary Perspective: Living Polymerization—Emphasizing the Molecule in Macromolecules. *Macromolecules* **2017**, *50*, 6979–6997.
- (2) Pelras, T.; Mahon, C. S.; Nonappa, I.; Kkalla, O.; Gröschel, A. H.; Müllner, M. Polymer Nanowires with Highly Precise Internal Morphology and Topography. *J. Am. Chem. Soc.* **2018**, *140*, 12736–12740.
- (3) Boyer, C.; Bulmus, V.; Davis, T. P.; Ladmiral, V.; Liu, J.; Perrier, S. Bioapplications of RAFT Polymerization. *Chem. Rev.* **2009**, *109*, 5402–5436.
- (4) Pan, X.; Tasdelen, M. A.; Laun, J.; Junkers, T.; Yagci, Y.; Matyjaszewski, K. Photomediated controlled radical polymerization. *Prog. Polym. Sci.* **2016**, *62*, 73–125.
- (5) Chen, M.; Zhong, M.; Johnson, J. A. Light-Controlled Radical Polymerization: Mechanisms, Methods, and Applications. *Chem. Rev.* **2016**, *116*, 10167–10211.
- (6) Anastasaki, A.; Nikolaou, V.; Zhang, Q.; Burns, J.; Samanta, S. R.; Waldron, C.; Haddleton, A. J.; McHale, R.; Fox, D.; Percec, V.; Wilson, P.; Haddleton, D. M. Copper(II)/Tertiary Amine Synergy in Photoinduced Living Radical Polymerization: Accelerated Synthesis of  $\omega$ -Functional and  $\alpha,\omega$ -Heterofunctional Poly(acrylates). *J. Am. Chem. Soc.* **2014**, *136*, 1141–1149.
- (7) Ribelli, T. G.; Konkolewicz, D.; Bernhard, S.; Matyjaszewski, K. How are Radicals (Re)Generated in Photochemical ATRP? *J. Am. Chem. Soc.* **2014**, *136*, 13303–13312.
- (8) Tasdelen, M. A.; Uygün, M.; Yagci, Y. Photoinduced Controlled Radical Polymerization in Methanol. *Macromol. Chem. Phys.* **2010**, *211*, 2271–2275.
- (9) Mosnáček, J.; Ilčíková, M. Photochemically Mediated Atom Transfer Radical Polymerization of Methyl Methacrylate Using ppm Amounts of Catalyst. *Macromolecules* **2012**, *45*, 5859–5865.
- (10) Pan, X.; Malhotra, N.; Dadashi-Silab, S.; Matyjaszewski, K. A Simplified Fe-Based PhotoATRP Using Only Monomers and Solvent. *Macromol. Rapid Commun.* **2017**, *38*, No. 1600651.
- (11) Dadashi-Silab, S.; Pan, X.; Matyjaszewski, K. Photoinduced Iron-Catalyzed Atom Transfer Radical Polymerization with ppm Levels of Iron Catalyst under Blue Light Irradiation. *Macromolecules* **2017**, *50*, 7967–7977.
- (12) Discekici, E. H.; Anastasaki, A.; Read de Alaniz, J.; Hawker, C. J. Evolution and Future Directions of Metal-Free Atom Transfer Radical Polymerization. *Macromolecules* **2018**, *51*, 7421–7434.
- (13) Treat, N. J.; Sprafke, H.; Kramer, J. W.; Clark, P. G.; Barton, B. E.; Read de Alaniz, J.; Fors, B. P.; Hawker, C. J. Metal-Free Atom Transfer Radical Polymerization. *J. Am. Chem. Soc.* **2014**, *136*, 16096–16101.
- (14) Lewis-Borrell, L.; Sneha, M.; Bhattacharjee, A.; Clark, I. P.; Orr-Ewing, A. Mapping the multi-step mechanism of a photoredox catalyzed atom-transfer radical polymerization reaction by direct observation of the reactive intermediates. *Chem. Sci.* **2020**, *11*, 4475–4481.
- (15) Liu, X.; Xu, Q.; Zhang, L.; Cheng, Z.; Zhu, X. Visible-light-induced living radical polymerization using in situ bromine-iodine transformation as an internal boost. *Polym. Chem.* **2017**, *8*, 2538–2551.
- (16) Sarkar, J.; Xiao, L.; Goto, A. Living Radical Polymerization with Alkali and Alkaline Earth Metal Iodides as Catalysts. *Macromolecules* **2016**, *49*, 5033–5042.
- (17) Li, S.; Han, G.; Zhang, W. Photoregulated reversible addition–fragmentation chain transfer (RAFT) polymerization. *Polym. Chem.* **2020**, *11*, 1830–1844.
- (18) Keddie, D. J.; Moad, G.; Rizzardo, E.; Thang, S. H. RAFT Agent Design and Synthesis. *Macromolecules* **2012**, *45*, 5321–5342.
- (19) Bergerbit, C.; Fariás-Mancilla, B.; Seiler, L.; Monteil, V.; Harrison, S.; D'Agosto, F.; Destarac, M. Synthesis of PMMA-based block copolymers by consecutive irreversible and reversible addition–fragmentation chain transfer polymerizations. *Polym. Chem.* **2019**, *10*, 6630–6640.
- (20) Kwak, Y.; Nicolaÿ, R.; Matyjaszewski, K. Synergistic Interaction Between ATRP and RAFT: Taking the Best of Each World. *Aust. J. Chem.* **2009**, *62*, 1384–1401.
- (21) Wager, C. M.; Haddleton, D. M.; Bon, S. A. F. A simple method to convert atom transfer radical polymerization (ATRP) initiators into reversible addition fragmentation chain-transfer (RAFT) mediators. *Eur. Polym. J.* **2004**, *40*, 641–645.
- (22) Stache, E. E.; Kottisch, V.; Fors, B. P. Photocontrolled Radical Polymerization from Hydridic C–H Bonds. *J. Am. Chem. Soc.* **2020**, *142*, 4581–4585.
- (23) Prier, C. K.; Rankic, D. A.; MacMillan, D. W. C. Visible Light Photoredox Catalysis with Transition Metal Complexes: Applications in Organic Synthesis. *Chem. Rev.* **2013**, *113*, 5322–5363.
- (24) Narayanan, J. M. R.; Tucker, J. W.; Stephenson, C. R. J. Electron-Transfer Photoredox Catalysis: Development of a Tin-Free Reductive Dehalogenation Reaction. *J. Am. Chem. Soc.* **2009**, *131*, 8756–8757.
- (25) Ischay, M. A.; Anzovino, M. E.; Du, J.; Yoon, T. P. Efficient Visible Light Photocatalysis of [2+2] Enone Cycloadditions. *J. Am. Chem. Soc.* **2008**, *130*, 12886–12887.
- (26) Hakobyan, K.; Gegenhuber, T.; McErlean, C. S. P.; Müllner, M. Visible-Light-Driven MADIX Polymerisation via a Reusable, Low-



Cost, and Non-Toxic Bismuth Oxide Photocatalyst. *Angew. Chem., Int. Ed.* **2019**, *58*, 1828–1832.

(27) Riente, P.; Pericàs, M. A. Visible Light-Driven Atom Transfer Radical Addition to Olefins using Bi<sub>2</sub>O<sub>3</sub> as Photocatalyst. *ChemSusChem* **2015**, *8*, 1841–1844.

(28) Whitfield, R.; Truong, N. P.; Messmer, D.; Parkatzidis, K.; Rolland, M.; Anastasaki, A. Tailoring polymer dispersity and shape of molecular weight distributions: methods and applications. *Chem. Sci.* **2019**, *10*, 8724–8734.

(29) Li, Y.; Qian, H.-J.; Lu, Z.-Y. The influence of one block polydispersity on phase separation of diblock copolymers: The molecular mechanism for domain spacing expansion. *Polymer* **2013**, *54*, 3716–3722.

(30) Ye, X.; Sridhar, T. Effects of the Polydispersity on Rheological Properties of Entangled Polystyrene Solutions. *Macromolecules* **2005**, *38*, 3442–3449.

(31) Lynd, N. A.; Hillmyer, M. A. Influence of Polydispersity on the Self-Assembly of Diblock Copolymers. *Macromolecules* **2005**, *38*, 8803–8810.

(32) Barth, J.; Buback, M.; Meiser, W.; Vana, P. Easy Access to the RAFT Equilibrium Constant. *Macromolecules* **2010**, *43*, 51–54.

(33) Whitfield, R.; Parkatzidis, K.; Truong, N. P.; Junkers, T.; Anastasaki, A. Tailoring Polymer Dispersity by RAFT Polymerization: A Versatile Approach. *Chem* **2020**, *6*, 1340–1352.

(34) Pelegri-O'Day, E. M.; Lin, E.-W.; Maynard, H. D. Therapeutic Protein–Polymer Conjugates: Advancing Beyond PEGylation. *J. Am. Chem. Soc.* **2014**, *136*, 14323–14332.

(35) Larnaudie, S. C.; Brendel, J. C.; Jolliffe, K. A.; Perrier, S. pH-Responsive, Amphiphilic Core–Shell Supramolecular Polymer Brushes from Cyclic Peptide–Polymer Conjugates. *ACS Macro Lett.* **2017**, *6*, 1347–1351.

(36) De, P.; Li, M.; Gondi, S. R.; Sumerlin, B. S. Temperature-Regulated Activity of Responsive Polymer–Protein Conjugates Prepared by Grafting-from via RAFT Polymerization. *J. Am. Chem. Soc.* **2008**, *130*, 11288–11289.

(37) Chen, C.; Richter, F.; Guerrero-Sanchez, C.; Traeger, A.; Schubert, U. S.; Feng, A.; Thang, S. H. Cell-Penetrating, Peptide-Based RAFT Agent for Constructing Penetration Enhancers. *ACS Macro Lett.* **2020**, *9*, 260–265.

(38) Olson, R. A.; Korpusik, A. B.; Sumerlin, B. S. Enlightening advances in polymer bioconjugate chemistry: light-based techniques for grafting to and from biomacromolecules. *Chem. Sci.* **2020**, *11*, 5142–5156.

(39) Peeler, J. C.; Woodman, B. F.; Averick, S.; Miyake-Stoner, S. J.; Stokes, A. L.; Hess, K. R.; Matyjaszewski, K.; Mehl, R. A. Genetically Encoded Initiator for Polymer Growth from Proteins. *J. Am. Chem. Soc.* **2010**, *132*, 13575–13577.

(40) Murata, H.; Carmali, S.; Baker, S. L.; Matyjaszewski, K.; Russell, A. J. Solid-phase synthesis of protein-polymers on reversible immobilization supports. *Nat. Commun.* **2018**, *9*, No. 845.

(41) Theodorou, A.; Liarou, E.; Haddleton, D. M.; Stavrakaki, I. G.; Skordalidis, P.; Whitfield, R.; Anastasaki, A.; Velonia, K. Protein-polymer bioconjugates via a versatile oxygen tolerant photoinduced controlled radical polymerization approach. *Nat. Commun.* **2020**, *11*, No. 1486.